Aerosol analysis by micro Laser-Induced Breakdown Spectroscopy: a new protocol for particulate matter characterization in filters

César Marina-Montes[a], Vincent Motto-Ros[b], Luis Vicente Pérez-Arribas[c], Jesús Anzano[a], María Millán-Martínez[d] and Jorge O. Cáceres[c*]

a Laser Lab, Chemistry & Environment Group, Department of Analytical Chemistry, Faculty of Sciences, University of Zaragoza. Pedro Cerbuna 12, 50009 Zaragoza, Spain

b Institut Lumière Matière, UMR5306 Université de Lyon 1 – CNRS, Université de Lyon, Villeurbanne, cedex 69622, France

c Laser Chemistry Research Group, Department of Analytical Chemistry, Faculty of Chemistry, Complutense University of Madrid. Plaza de Ciencias 1, 28040 Madrid, Spain

d Associate Unit CSIC-University of Huelva "Atmospheric Pollution", Center for Research in Sustainable Chemistry-CIQSO, Campus El Carmen s/n, 21071 Huelva, Spain

Abstract:

Atmospheric aerosols (particulate matter – PM) affect the air quality and climate, even in remote areas, such as the Antarctic Region. Current techniques for continuous PM monitoring are usually complex, costly, time consuming and do not provide real-time measurements. In this work, based on micro laser-induced breakdown spectroscopy (LIBS), an innovative method with an optical design and multi-elemental scanning imaging, is presented to characterize PM collected in filters from Antarctica. After following a simple protocol and under atmospheric pressure, the new approach allows to obtain a global visualization of the elemental PM composition of the filters with a minimum sample destruction and preparation. For the first time, we were able to map the localization of pollutants in filters at high spatial resolution and speed. This recent method offers a new insight on the characterization of PM, particularly in isolated areas, where no complex equipment and real time measurements are demanded.

Keywords: Laser-induced breakdown spectroscopy, filter characterization, Atmospheric aerosols, micro LIBS imaging, Antarctica.

1. Introduction

Aerosol particulate matter (PM) is a key component in the atmosphere. These particles have sizes ranging from nanometres to micrometres and act as climate drivers, influencing the earth´s radiative budget [1-4] as well as the cloud structure [5, 6] and formation [7]. Depending on the meteorological conditions, aerosols are able to travel thousands of kilometres [8], reaching remote and isolated places, such as Antarctica [9, 10]. Their typical lifetime in the troposphere range from hours to weeks [11], having an effect on air quality [12, 13] and consequently, on human health [14-17] and the environment [18, 19]. These human and environmental effects mainly depends on the particle chemical composition and size distribution. Ambient air aerosol particles are formed by a complex mixture of single particles internally composed of various elements [20], with different composition, physical properties and size depending on their natural (sea salt, volcanoes, crustal dust, etc.) or anthropogenic (fossil fuel combustion, agriculture, etc.) sources. Among others, chemical components include trace metals, sea salts and crustal elements. Thus, since there is a wide range of aerosol composition and size, knowledge of aerosol content is necessary when studying their potential sources and impacts on the environment [21-23], as well as to mitigate these impacts [4].

The analysis of PM filter samples is commonly used worldwide in environmental aerosol monitoring. The European Standard (EN12341:2015) gives requirements for the collection of suspended PM on filters as well as limit concentrations in ambient air for PM_{10} and $PM_{2.5}$. Traditional analytical techniques for the determination of the elemental aerosol filter composition include X-ray Fluorescence Spectroscopy (XRF) [24], Inductively Coupled Plasma-Optical Emission Spectroscopy (ICP-OES) [25] and/or Inductively Coupled Plasma-Mass Spectrometry (ICP-MS) [23]. Despite the fact these

techniques offer high performances, they generally require complex instruments and have limitations for doing daily routine laboratory measurements and provide global analysis. Although being an analytical challenge due to its wide variation in aerosol particles [26], the full visualization of PM internal composition is demanded to better comprehend PM potential sources and interactions. This is particularly the case of our Antarctic PM filters, with an expected low PM concentrations compared to urban areas. Hence, chemical characterization of single particles through imaging methods represent a highly valuable approach to globally visualize the single internal PM composition. In this work, an elemental imaging technique for characterizing PM_{10} collected on quartz fiber filters, based on micro laser-induced breakdown spectroscopy (LIBS) has been developed. This technique, with ppm-level detection and a resolution of up to 10 μm, is suitable with common microscopy instruments for imaging and determining elemental distributions in PM filter samples. LIBS is a functional technique used for multiple applications [27-29] and ideal when field work is needed [30]. By applying LIBS to PM filter samples, over the study area, the individual optical responses from the inorganic elements contained in the filters are obtained creating an elemental map formed by pixels within a reasonable time period. One of the main LIBS advantages include the high working speed compared to other techniques. LIBS applications to aerosol analysis have been reported previously [26, 31-33], however, to the best of our knowledge, we were the first to demonstrate LIBS scanning microanalysis potential use for characterizing ambient air aerosol particles deposited on filters.

In this study, we present the feasibility of employing micro LIBS imaging for the characterization of PM_{10} on filters. The only requirement for the elemental imaging of the filters is a flat and uniform surface, which is obtained following the new protocol we describe. This method gives the possibility of an automated, fast and multi-elemental

analysis of aerosol filter samples working in ambient atmosphere and with minimum destruction of the samples. For conducting this feasibility, PM filters collected in Antarctica were studied. It is important to point out that this isolated collection site requires high sensitivity since the expected PM elemental concentrations are very low. Our results provide advanced insights into the employment of LIBS imaging in environmental monitoring of suspended PM in ambient air.

2. Methods

2.1 Sample collection

Ambient air aerosol particles were collected in the 2018/2019 and 2019/2020 Spanish Antarctic campaigns at the surroundings of the Spanish Antarctic Research stations "Gabriel de Castilla" on Deception Island (62°58′09″S, 60°42′33″W) and "Juan Carlos I" on Livingston Island (Queen Sofía Mount - 275 m high: 62º40'8.5"S, 60º22'50.1"W). Both islands are located approximately 120 km north of the Antarctic Peninsula and are part of the volcanic South Shetland Archipelago.

A total of 10 and 28 samples were collected in the austral summer (from December to March) of 2018–2019 & 2019-2020, respectively. Each sample was collected during 72 h period. PM samples were collected in circular quartz microfiber filter papers of 150 mm diameter (Pallflex) through a Digitel DHA-80 high-volume sampler (30.6 m^3/h). In order to avoid external particle contamination, filters were meticulously manipulated using tweezers and nitrile globes. Additionally, filters were stored before and after PM sampling in aluminium foil. Once in the lab, mass concentration of each sample was obtained by gavimetry following the standard gravimetric measurement method (EN12341:2015) [37]. All of the samples were analysed by micro LIBS, while some samples (2019-2020

campaign) were analysed by both, LIBS & ICP OES-MS. Importantly, although a large number of samples were collected and analysed, just a few of them were required and presented on this study to develop the new protocol.

2.2 ICP OES-MS

After obtaining PM10 mass concentration, nine filters were treated following a procedure specifically described elsewhere [38]. A 3/16 fraction (~33.12 cm^2) of each filter was acid digested (2.5 mL HNO_3: 5 mL HF: 2.5 mL $HClO_4$) for the analysis of major and trace elements by ICP-OES (Agilent model 5110) and ICP-MS (Agilent model 7900), respectively. For quality assurance and control, analysis of blank filters and the NIST-1663b (fly ash, Reference Standard Material) were implemented. External calibration was performed in ICP-MS by using cocktail solutions (0.25, 0.5, 1, 2, 5 and 10 ppb as well as a HNO_3 5% blank). ^{103}Rh was used as internal standard with the objective of minimizing the possible fluctuations of the plasma. External calibration was performed in ICP-OES using elemental standards solutions (0.05, 0.5, 1, 2, 5, 10, and 25 ppm and a HNO_3 5% blank). The limits of detection (LoD) obtained for most of the elements were in the range from 0.01 to 11 ng/m^3 for ICP-MS, and 1.5 ng/m^3 to 1.85 $\mu g/m^3$ for ICP-OES.

2.3 Experimental setup and data acquisition

The micro LIBS instrumental setup has been previously described in detail elsewhere [34-36, 39] . Briefly explained, a Q-switched Nd:YAG laser (Centurion GRM, Quantel) working at 1064 nm, with a pulse duration of 8 ns, 8 μm beam diameter and a repetition rate of 100 Hz, was used for plasma creation. The laser pulse was vertically focused onto the PM filter by a 15x magnification objective (LMM-15X-P01, Thorlabs). The spot size

was fixed and the typical crater size was in the range of 6-7 μm. The instrument was equipped with a motorized translation 3-axis (XYZ) stage, allowing the sample during the analysis to automatically travel to up a 50 mm distance. Plasma light was collected by two independent systems. The first system was composed by a Czerny-Turner spectrometer (Shamrock 303, Andor Technology), allowing the direct injection of the plasma light for an optimal sensitivity in the 200 nm range. The second system was an optical system composed by a quartz lens and fiber bundle connected to a Czerny-Turner spectrometer (Shamrock 500, Andor Technology). Both spectrometers were assembled with intensified charge-coupled device (ICCD) cameras (iStar, Andor Technology) set to 1200 l/mm (Shamrock 303i) and 600 l/mm (Shamrock 500i) gratings. Both cameras were synchronized with the Q-switch of the laser, using a delay of 1 μs and a gate of 5 μs. The width of the entrance slit of the spectrometers Shamrock 303i and Shamrock 500i was set to 50 μm and 35 μm, respectively. Particularly in our study, the spectrometer 303 was configured in the spectral range 180–253 nm to detect, among others, C, P, Zn, Si; while the spectrometer 500 was configured in the spectral range 290–379 nm to detect some other elements of interest, such as, Si, Fe, Al, Ca, Ti and Na. Laser output energy was set to 1.5 mJ. The measurements were conducted with an argon flow of 0.8 l/min flowing the plasma region. Homemade software elaborated in LabVIEW environment governed the full process and allowed to automatically obtain, at particular lateral resolution, scanned sequences of the PM filter samples. For most of the experiments presented below, a 300x100 (15 mm x 5 mm) sequence was implemented, covering a surface of 75 mm^2. The global time (sample preparation + LIBS experiment) for the analysis of a single filter was 10 minutes, while the duration of each LIBS experiment (a full map of ~30,000 spectra) was approximately 5 minutes.

2.4 LIBS processing

The intensity of each measurement site and of each species of interest was extracted by an advanced spectrum treatment [40, 41]. Firstly, an emission line was chosen for each element of interest. The selection of the emission lines was based on two aspects: (1) Only the strongest line of each element in the probed range was selected, and (2) The selected line should be free from interferences from other elements. Secondly, the algorithm specified a baseline fit through the use of a polynomial function and subtracted it from the emission signal. Thirdly, a 2D matrix, displayed as an image using a false-color scale, was presented for each species. This matrix contains on each cell (i.e. pixel) the intensity signal from a point on the surface for the given element. And finally, the images associated to each species were processed using ImageJ software (NIH, Bethesda, MD, www.nih.gov).

Two values were then extracted from each elemental image; the average and accumulated signal associated to each element. First to obtain the accumulated signal, all the intensities of a given line were sum if higher than 3 times the background noise (measured on single shot spectra). Then to obtain the average signal, those accumulated intensities were divided by the number of pixels constituting the sequence.

3. Results and discussion

3.1 Validation of sample preparation protocol

It is important to emphasize that to collect PM particles, air monitoring filters are made on the top side of quartz microfibers, while the bottom side is made of two layers of quartz paper. In this way, during the PM collection through the samplers, the microfibers are face up in order to allow PM particles to be deposited in the filters.

Since filter papers are made of quartz microfibers, one challenging task in LIBS PM filter microanalysis is achieving an optimal spectral signal, distinct to Si, of the different single particles contained in the filters. To date, previous LIBS PM filter analysis were implemented directly over the filter surface, without following any sample preparation methodology [33, 42, 43]. Therefore, to determine the best sample preparation which maximizes the PM elemental signal in a micro LIBS imaging configuration, two different protocols were compared, a traditional one (no-preparation) and a developed one (preparation). Fig. 1 shows a schematic representation of the single steps of each protocol. The two protocols are described as follows: Firstly, on both cases, double sided tape was placed in a microscope glass slide. Secondly, a small piece (about 16 mm x 6 mm) of the same PM filter (Fig. 1a) was cut. The quartz microfiber surface composition of the filter is shown in Fig. 1b. Thirdly, the filter piece was adhered facing up (Fig. 1c; no-preparation sample) or facing down (Fig. 1d; preparation sample) to the double side tape. Fourthly, in the interest to better adhere the PM to the tape, a force was applied through a weight over the preparation sample (76.6 g/cm^2) for a brief period of time (~15 seconds). Since this force was practiced over the quartz paper side, no contact contamination to the PM particles was possible. And finally, the quartz paper layers of the preparation sample were removed using tweezers. It is important to point out that in the no-preparation protocol, the filter surface is not flat because of the disposition of the quartz fibers (Fig. 1e), which makes difficult to control the mastering of the laser ablation. Thus, it is not possible to control perfectly the focus position of the laser beam. On the contrary, since the surface is flat in the preparation protocol (Fig. 1f), the mastering of the laser ablation is perfectly controlled.

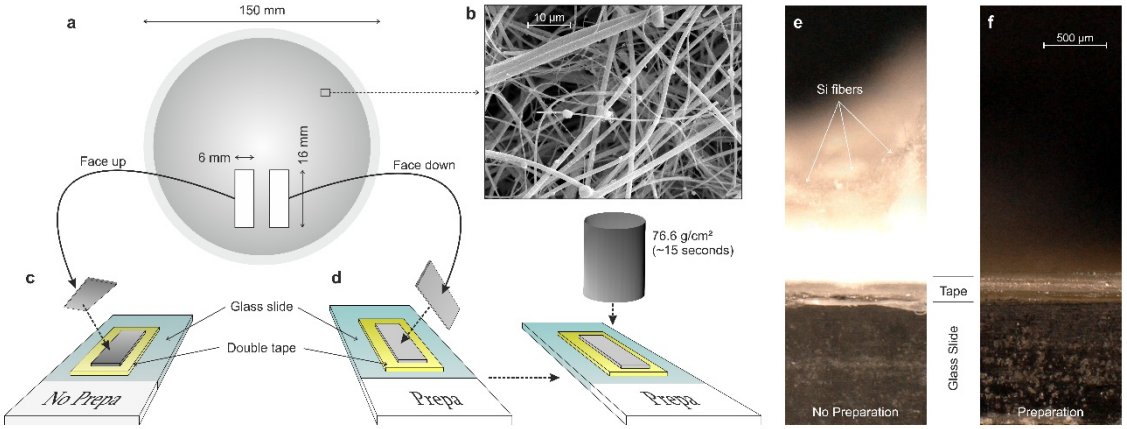

Figure 1. (a), Schematic representation of the cutting process of a small section of a PM filter sample. (b), Scanning electron microscopy (SEM) image of stack Antarctic PM on a quartz microfiber filter. (c), Face up PM filter adhesion following the no-preparation protocol. (d), Face down PM filter adhesion and force application following the preparation protocol. (e), Microscope image of a no-prepared filter sample after micro-LIBS analysis. (f), Microscope image of a prepared filter sample after micro-LIBS analysis.

In order to validate the proposed preparation protocol, LIBS microanalysis was performed on both samples, as well as on a prepared control one. Control samples were handled and stored in the same way as the PM measurement filters. Fig. 2 shows the imaging results obtained in the different cases. Fig. 2a illustrates the elemental images obtained for Si (288.14 nm) and Ti (334.94 nm) corresponding to the three different scenarios (no-preparation, preparation and preparation control sample). These elemental images were obtained with a lateral resolution of 50 µm. Because filters are made of quartz, the Si signal is distributed in all of the samples. However, Si signal is more intense on the preparation and control samples compared to the no-preparation sample. Additionally, despite the fact that Si is a constituent of the filter material, Si particles are detected in the preparation protocol as can be seen by the different intensity levels. In the case of Ti, which is a constitutive element of crustal soils, its signal was homogeneously distributed in the preparation sample. Nevertheless, there is no Ti signal in the no-preparation and control samples, except some impurities (Fig. 2a).

Fig. 2b shows the average LIBS signal associated to some representative elements in the three scenarios. As it can be seen, the average signal difference between the scenarios is clearly notable for the majority of the elements such as Ca (317.93 nm), Fe (302.30 nm), Ti (334.94 nm) and Mn (294.92 nm), being this of at least several orders of magnitude. However, this difference is markedly lower for Si and slightly lower for Al (309.27 nm) and Na (330.23 nm). Concerning these differences, Si content in the blank filter is explained again by the composition of the filter itself, while Al content by the use of aluminium foil. This kind of foil is commonly used for transporting filters and avoiding particle contamination from external sources. Furthermore, the strong Na signal associated to the no preparation scenario may be explained by the low excitation level of this element. Therefore, Na emission is barely affected by the ablation efficiency. Finally, since there are almost two orders of magnitude between the preparation and no-preparation protocol for Na and Al, it is possible to take them into account in the analyses. On the contrary, it is impossible to consider Si particles.

As seen in Fig. 2c and based on the elemental lines obtained with the two spectrometers, some previous elements were identified on the preparation protocol. Some of these elements, such as Fe (302.30 nm), Ca (317.93 & 373.69 nm) and Ti (323.45 & 334.94 nm), are not detected in the non-preparation scenario. Additionally, the signal intensities of Al (309.27 nm) and Na (330.23 nm) associated to the non-preparation sample are very low compared to the preparation protocol. Since C (193.09 nm) is a constituent of the material of the filters, it signals appears on all the scenarios. Furthermore, micro LIBS analysis over just the double tape (with no filter adhered) revealed no additional elements except carbon. Overall, these results clearly show the importance of the preparation protocol, allowing to detect elemental signals ignored by the no-preparation protocol. It

should be noted that any element present naturally in the filter material or in the double tape should not be taken into consideration for the analyses as it is the case for C and Si.

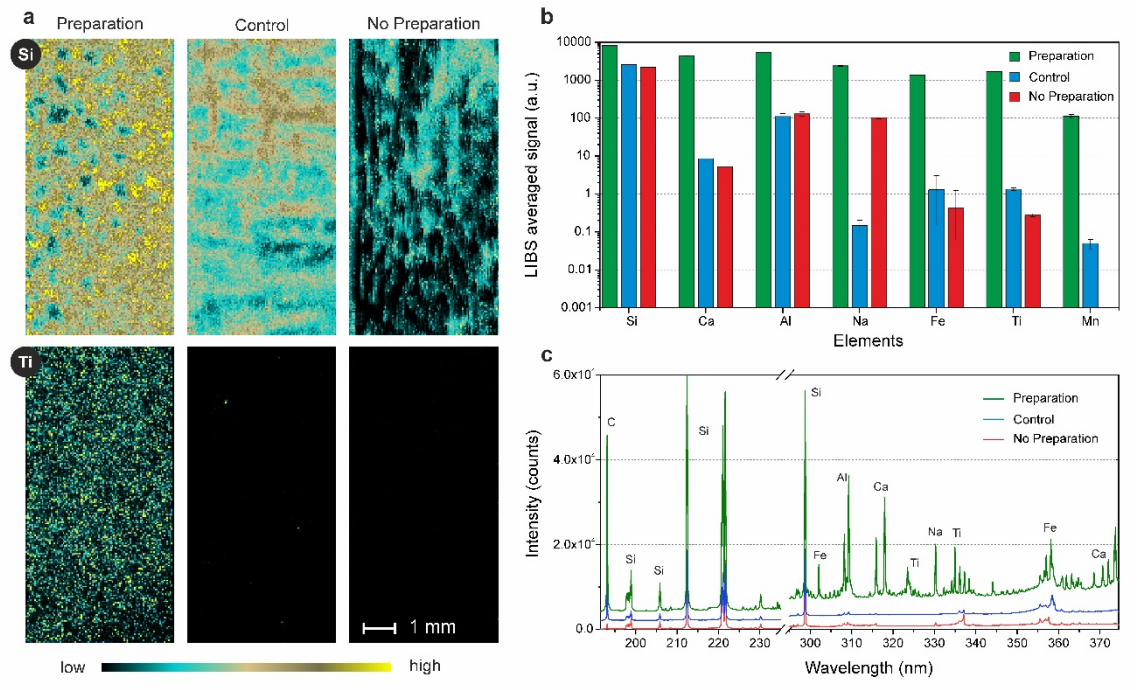

Figure 2. (a), Distribution imaging of Si and Ti in a PM filter sample (preparation/no preparation) and in a prepared control sample. The images were obtained using a pulse energy of 3 mJ, a 50-µm resolution and represent 30,000 pixels. (b), Average LIBS signal associated to some representative elements for the three different scenarios (preparation/control/no preparation). (c), Average LIBS spectrum corresponding to the three scenarios in two spectral ranges 180–253 nm and 290–379 nm.

3.2 Lateral resolution

Although the use of the preparation protocol shows considerable advances in the signal detection compared with the no preparation methodology; a good balance between the spatial resolution and the signal intensity is necessary. It should be emphasized that laser ablation is a violent process due to it is accompanied by different mechanisms, such as shock wave formation and thermal diffusion through the sample. In the case of fragile material, these effects might cause much more sample deterioration than caused by the ablation itself. In the present case, (particles distributed on filter), using a high lateral resolution (distance between two consecutive laser shots) may lead to a loss of

information (under sampling). For example, a particle might be between two ablation site and therefore not taken into account in the signal. In the other case, a too low lateral resolution may be critical since the shock wave and/or thermal diffusion may have pushed or destroyed the neighbouring ablation sites creating artefact in the analysis and bias in the extracted signal (we can call it by analogy over sampling). This will be especially critical if the particles are not adhering well to the filter fibers. Therefore, considering all of these concerns associated to the laser ablation process, there is an optimal step size value to find. Our idea was to start to high resolution (100 µm) and check eventual signal deterioration when reducing the step size.

To this aim we employed different measurement resolutions; 100, 75, 60, 50, 40, 25 and 10 µm, in different sections of the same 150 mm filter. The experimental results are shown in Fig. 3. At first glance, the distribution imaging of Si (288.14 nm) and Ti (334.94 nm) associated to the studied resolutions is given in Fig. 3a. It can be observed that for these two elements, the optimal step size is located between 40 and 60 µm. Fig. 3b exhibits how Ti (334.94 nm), Al (309.27 nm), Na (330.23 nm) and Si (298.76 nm) signals increased with increasing the resolution until reaching a maximum signal close to the 40 µm resolution value. Both, an excessively low and high resolution were unable to provide enough signal. An intermediate resolution was considered to be the best operating resolution for the LIBS microanalysis. Thereupon, a 40 µm resolution was chosen for posterior analysis.

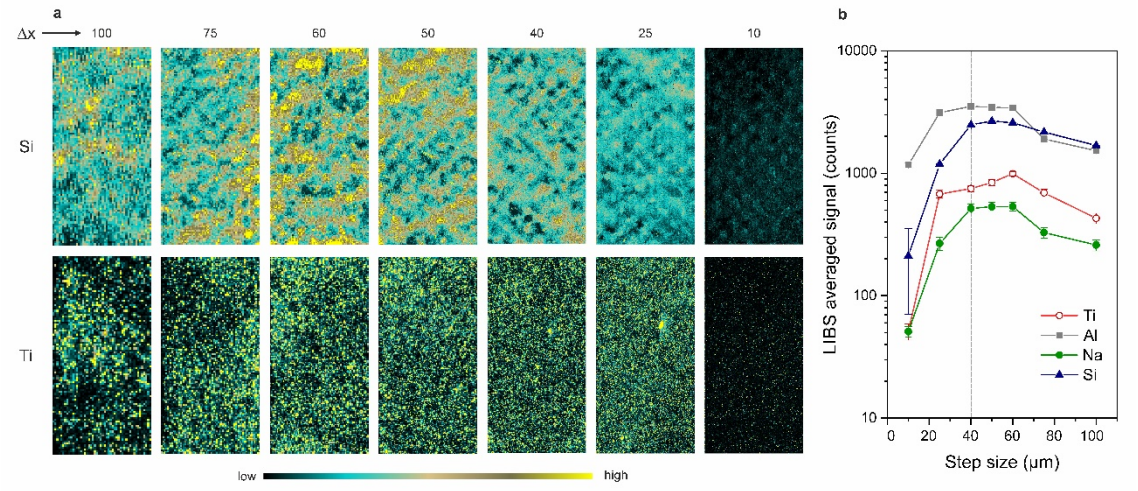

Figure 3. Resolution of LIBS microanalysis. (a), Elemental images of Si and Ti in the same PM filter sample, ranging from 100 (8,200 pixels) to 10 (751,000 pixels) µm resolution. (b), Mean Si and Ti LIBS signal as a function of the resolution (µm).

3.3 Representativeness

In order to test the representativeness of a single PM filter sample piece, LIBS imaging was applied to 3 longitudinal sections of the same 150 mm diameter PM filter sample. Three different LIBS images were obtained from this sample. All of the analysis were performed on the longitudinal axis of the filters (Fig. 4a) with a resolution of 40 µm. Each analysis covered a surface of 75.6 mm² (15 x 5.04 mm) and a total number of pixels of 48,132. For the three analyses, Al (309.27 nm), Ti (334.94 nm), Na (330.23 nm) and Cu (327.39 nm) spatial distribution images are shown in Fig. 4b. Note that for better clarity only the central regions of the images are shown in the figure 4b. The mean elemental signals for each three different spatial distribution images are represented in the graph of Fig. 4c. According to the graph, Al, Ti and Na are present in rather high content in all of the analysis, while Cu is present in a very low content. Additionally, this graph shows that Al, Ti and Na images are representative of all the filters, whereas Cu image is not. Therefore, it should be concluded that the distribution of representative elements in the filter, such as Al, Ti and Na, is homogeneous. This means that a unique longitudinal

section of the filter is sufficient in order to know the global representative elemental PM composition of it. However, although LIBS is able to detect single isolated particles, such as Cu particles, it should be taken into account that, due to the reduced number of particles, the distribution of minority elements observed in such LIBS image may be not representative of all the filter.

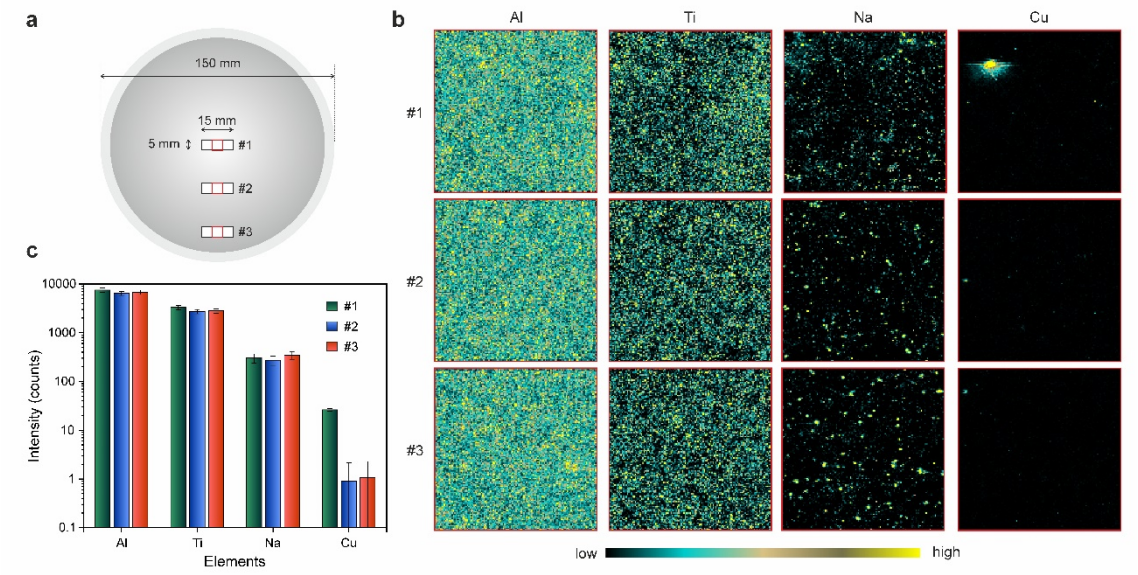

Figure 4. (a), Three different sections of the same 150 mm PM filter that were analysed. The total length and width of each section is similar and corresponds to 15 and 5,05 mm, respectively. The surface is 75.6 mm². (b), Spatial distribution images of Al, Ti, Na and Cu over 3 different sections of the filter at 40 µm resolution. Only the central regions are shown (red square in a). (c), Mean Al, Ti, Na and Cu LIBS signal for each different regions of the PM filter.

3.4 Calibration curves for ICP and LIBS

With the objective of validating through ICP some elements present in the filter, calibration curves were implemented. Nine PM filter samples were analysed by both, ICP (OES & MS) and LIBS. The micro LIBS analysis were conducted as described above (section of 75.6 mm² with a resolution of 40 µm) while the ICP analysis were conducted after dissolving the 3/16 surface of the filter (equivalent to ~3312 mm²). Calibration curves were then established using the accumulated LIBS signal and the retrieved ICP concentrations of each selected PM filters. As an example, it can be seen in Fig. 5 the

calibration curves for Ti (a) and Fe (b). These LIBS-ICP calibration curves shows a good linearity with a coefficient of determination of 0.996 and 0.988 for Ti and Fe, respectively. Thus, LIBS signal is proportional to the ICP mass concentration. This behaviour implies the possibility to develop quantitative measurements of representative elements with LIBS through ICP calibration.

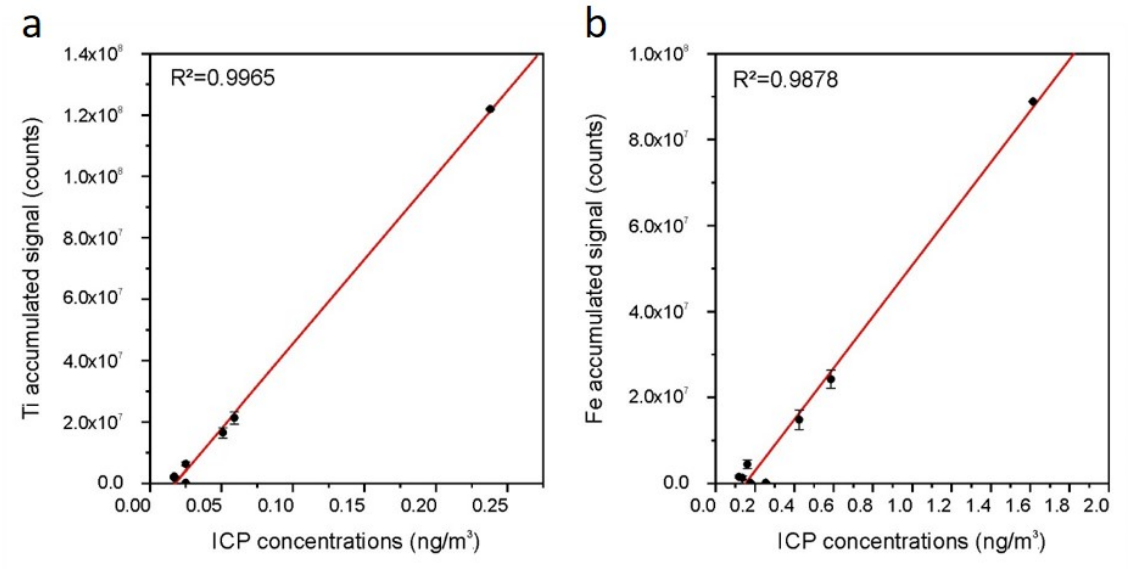

Figure 5. LIBS-ICP calibration curves for (a) Ti and (b) Fe.

From these calibration curves, it is also possible to evaluate the limit of detections of LIBS analysis, obtained in a single shot configuration. The calibration curves shown in figure 5 correspond to the accumulated signal of Ti and Fe on the LIBS and ICP analysed filter surfaces. The slope allows to determine, together with ICP and LIBS surfaces, the sensitivity S. The background noise of LIBS single shot measurements was evaluated to 250 counts. Using the general definition of the LoD:

$$LoD = \frac{3\sigma}{S} \quad (1)$$

where σ represents the standard deviation of the background noise and S the sensitivity, the obtained LoD values of LIBS analysis associated to Ti and Fe were $3.11E^{-08}$ and

$2.86E^{-07}$ ng/m^3, respectively. These LoD values of LIBS are lower than those obtained for the same elements using ICP-OES (5.25 ng/m^3 for Ti and 0.06 µg/m^3 for Fe). It is important to point out that for PM filter characterization, the LoD value is generally introduced as a function of the air volume that pass through the filter. These obtained low LoD values open the possibility to study much lower accumulation time for filters, instead of the normal 24 hours' accumulation period.

3.5 Exotic elements

In addition to rather common elements such as Al, Ti, Na, Fe, etc. many other elements, defined as exotic, were detected. Figure 6 represents a multicolour scale image of some exotic elements found in an individual PM filter sample. The spectra shown correspond to single shot spectra. As it can be seen on the figure, some elements are present, such as Ni, Zn, Cr, Ba, Cu and P, in six pixels of the image. These elements are probably associated to single particles and their quantification is not possible for two main reasons: (1) These elements are not detected with enough accuracy by ICP analysis, and/or (2) LIBS is not representative enough of the ICP due to the low number of particles and loss of representability (both analyses cannot be compared). However, it exists the possibility to observe P-based particles and address the composition of metallic particles. This is the case of Cr, which is probably related to a Fe alloy. The possibility of detect single particles by micro-LIBS imaging offers an extraordinary potential to study an extensive range of atmospheric processes, since multiple impacts of aerosols on climate are determined by the properties of the individual particles [44-46]. Additionally, the space-resolved capability offers the possibility to study the behaviour as well as the correlation between elements (composition of the particles) and between particles if they agglomerate (micro-nanoparticles at the size of the laser spot or larger than the LIBS resolution).

.

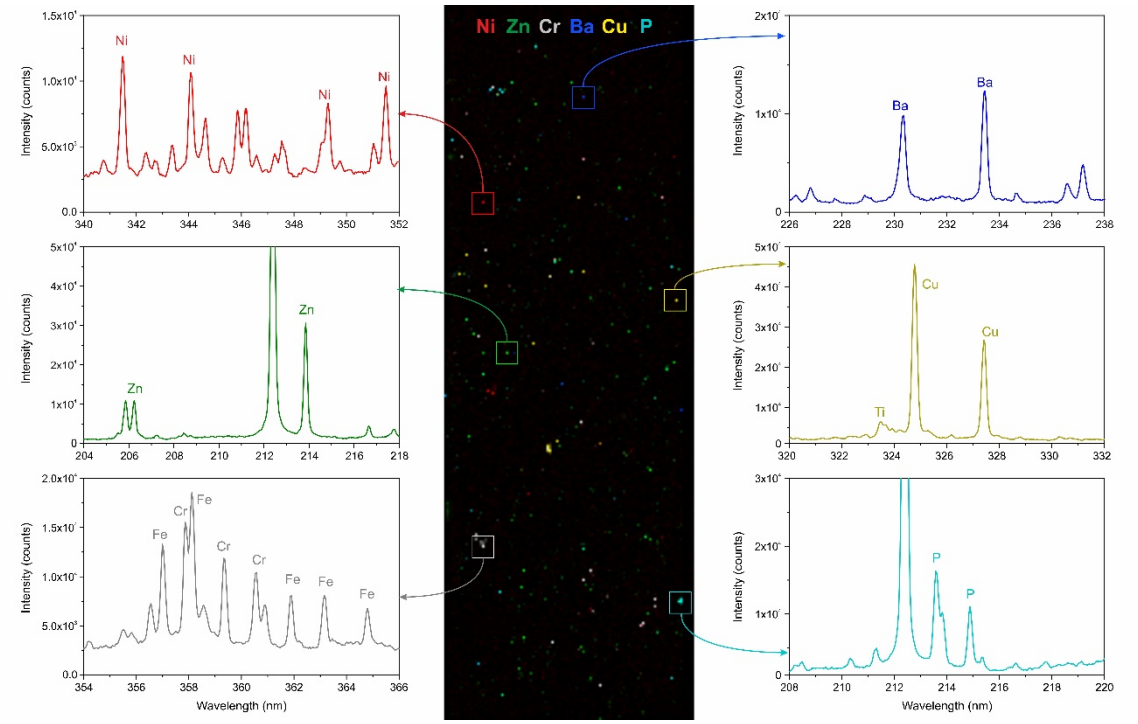

Figure 6. Multicolour spatial distribution image of some elements (Ni, Zn, Cr, Ba, Cu and P) in a PM filter sample. Each spectra accounts to a single shot.

3.6 Discussion

Results presented on the previous sections indicate that both LIBS and ICP-MS are powerful complementary techniques, particularly when validating LIBS results. Although ICP is the reference method, both techniques offer multiple advantages on the PM characterization of filters. Since the size of the particles is unknown, the limit of detection of LIBS is difficult to obtain. Nevertheless, based on our study, it should be mentioned that LIBS detection capability is great as well as its sensitivity. As an example, LIBS may be able to detect unique particles with a mass in the range of 10x1e-15 g (10 ppm of 1 ng, the latter is the typical mass ablated) while ICP may not. On the other hand, ICP may be able to detect a large number of smaller particles, while LIBS may not. This fact points out the importance of LIBS technique, adding additional information to the traditional ICP results. Furthermore, LIBS technique gives the possibility of obtaining

information from a small surface with almost no sample destruction, allowing to get a rapid visualization of the filter composition. Additional PM characterization techniques such as ICP, SEM or Raman will be employed on the PM filters aiming to full understand the composition of Antarctic aerosols.

The combination of micro LIBS and ICP opens the possibility to use filter with strong accumulation of particles for establishing our own calibration filters. Additionally, an extra option for elaborating these calibration curves on the near future would be the development of an instrument which would work with known amount of particles. In this study, we have not processed multi-face particles. Consequently, multivariate methods should be applied to evaluate and characterize the composition of the particles. Finally, the very fast analysis time and the quasi real time allowed by micro LIBS opens interesting perspectives for future air pollution monitoring systems.

4. Conclusion.

For the first time we have successfully demonstrated scanning microanalysis of PM filter samples using LIBS. Our team has developed an innovative, fast, multi-elemental method complementary to ICP capable to image PM in small section of filters at very low LoD. The final obtained analytical performance of micro LIBS analysis on filters is high in terms of sensitivity (ppm-level), lateral resolution (40 μm) and operating speed (100 Hz). This performance is similar to other LIBS imaging studies developed by our research group [34-36]. Firstly, the use of a preparation protocol allowed to obtain the maximum number of elemental signals compared to the non-preparation procedure. Secondly, 40 μm was selected as the best operating resolution for PM filters after using a resolution ranging from 10 to 100 μm. Thirdly, the spatial distribution of PM was studied in three different sections of the same filter in order to know its representativeness. Since the elemental distribution of some representative elements resulted to be homogeneous in all

of the sections with no significate signal differences, the analysis of just one section of the filter was necessary for obtaining a global PM composition of representative elements. Fourthly, Ti and Fe LIBS signals were validated trough LIBS-ICP calibration curves. And finally, single shot spectra analysis of individual particles revealed some exotic elements, such as Ni, Zn, Cr, Ba, Cu and P.

LIBS elemental microanalysis of PM has a considerable potential for characterization of aerosol on filters. The technique gives the possibility of automated analysis of aerosols in quasi-real-time without any further treatment. Furthermore, it allows to localize trace elements as well as their distribution over the Antarctic studied area.

Declaration of competing interest

The authors declare no conflict of interest

Acknowledgements

The authors gratefully acknowledge the following institutions for facilities and material resources: University of Zaragoza (Spain), Complutense University of Madrid (Spain) and Institut Lumière Matière (University of Lyon 1 – CNRS, France). The contribution from Jesús de la Rosa from the Associate Unit "Atmospheric Pollution" (CSIC-University of Huelva, Spain) is also appreciated. This project forms part of the Spanish Ministry of Science research program (CTM2017-82929-R & PID2020-112570RB-C21) in collaboration with the Government of Aragon proposal E23_17D and E49_20R. CMM's work was funded through a predoctoral contract (FPI) granted by the Spanish Government. Financial support from the European Social Fund & University of Zaragoza is acknowledged. The authors thank the ET at the Gabriel de Castilla Spanish Antarctic research station and Javier del Valle Melendo (CUD- University of Zaragoza) for help with the installation of equipment and sample collection during the Antarctic campaign 2018/2019. The UTM and Juan Carlos I Spanish Antarctic research station staff are

acknowledged for their enormous support during the Antarctic campaign 2019/2020 (specially Hilo Moreno and Joan Riba).

References:

[1] I.E. Nielsen, H. Skov, A. Massling, A.C. Eriksson, M. Dall'Osto, H. Junninen, N. Sarnela, R. Lange, S. Collier, Q. Zhang, C.D. Cappa, J.K. Nøjgaard, Biogenic and anthropogenic sources of aerosols at the High Arctic site Villum Research Station, Atmos. Chem. Phys., 19 (2019) 10239-10256.

[2] IPCC, Climate Change 2013: The Physical Science Basis. Contribution of Working Group I to the Fifth Assessment Report of the Intergovernmental Panel on Climate Change, Cambridge University Press, Cambridge, United Kingdom and New York, NY, USA, 2013.

[3] J. Fan, D. Rosenfeld, Y. Zhang, S.E. Giangrande, Z. Li, L.A.T. Machado, S.T. Martin, Y. Yang, J. Wang, P. Artaxo, H.M.J. Barbosa, R.C. Braga, J.M. Comstock, Z. Feng, W. Gao, H.B. Gomes, F. Mei, C. Pöhlker, M.L. Pöhlker, U. Pöschl, R.A.F. de Souza, Substantial convection and precipitation enhancements by ultrafine aerosol particles, Science, 359 (2018) 411.

[4] M. Descheemaecker, M. Plu, V. Marécal, M. Claeyman, F. Olivier, Y. Aoun, P. Blanc, L. Wald, J. Guth, B. Sič, J. Vidot, A. Piacentini, B. Josse, Monitoring aerosols over Europe: an assessment of the potential benefit of assimilating the VIS04 measurements from the future MTG/FCI geostationary imager, Atmos. Meas. Tech., 12 (2019) 1251-1275.

[5] S. Twomey, The Influence of Pollution on the Shortwave Albedo of Clouds, Journal of the Atmospheric Sciences, 34 (1977) 1149-1152.

[6] H. Zheng, S. Kong, F. Wu, Y. Cheng, Z. Niu, S. Zheng, G. Yang, L. Yao, Q. Yan, J. Wu, M. Zheng, N. Chen, K. Xu, Y. Yan, D. Liu, D. Zhao, T. Zhao, Y. Bai, S. Li, S. Qi, Intra-regional transport of black carbon between the south edge of the North China Plain and central China during winter haze episodes, Atmos. Chem. Phys., 19 (2019) 4499-4516.

[7] A.S. Ackerman, O.B. Toon, D.E. Stevens, A.J. Heymsfield, V. Ramanathan, E.J. Welton, Reduction of Tropical Cloudiness by Soot, Science, 288 (2000) 1042.

[8] M. Radojevic, V. N. Bashkin, Practical Environmental Analysis, RSC, Cambridge, 2006.

[9] Q.-H. Hu, Z.-Q. Xie, X.-M. Wang, H. Kang, P. Zhang, Levoglucosan indicates high levels of biomass burning aerosols over oceans from the Arctic to Antarctic, Scientific Reports, 3 (2013) 3119.

[10] F. Eisele, D.D. Davis, D. Helmig, S.J. Oltmans, W. Neff, G. Huey, D. Tanner, G. Chen, J. Crawford, R. Arimoto, M. Buhr, L. Mauldin, M. Hutterli, J. Dibb, D. Blake, S.B. Brooks, B. Johnson, J.M. Roberts, Y. Wang, D. Tan, F. Flocke, Antarctic Tropospheric Chemistry Investigation (ANTCI) 2003 overview, Atmospheric Environment, 42 (2008) 2749-2761.

[11] J.H. Seinfeld, S.N. Pandis, Atmospheric chemistry and physics: from air pollution to climate change, John Wiley & Sons, Inc., Hoboken, 2006.

[12] F. Dominici, M. Greenstone, C.R. Sunstein, Particulate Matter Matters, Science, 344 (2014) 257.

[13] S. Fuzzi, U. Baltensperger, K. Carslaw, S. Decesari, H. Denier van der Gon, M.C. Facchini, D. Fowler, I. Koren, B. Langford, U. Lohmann, E. Nemitz, S. Pandis, I. Riipinen, Y. Rudich, M. Schaap, J.G. Slowik, D.V. Spracklen, E. Vignati, M. Wild, M. Williams, S. Gilardoni, Particulate matter, air quality and climate: lessons learned and future needs, Atmos. Chem. Phys., 15 (2015) 8217-8299.

[14] M. Adam, T. Schikowski, A.E. Carsin, Y. Cai, B. Jacquemin, M. Sanchez, A. Vierkötter, A. Marcon, D. Keidel, D. Sugiri, Z. Al Kanani, R. Nadif, V. Siroux, R. Hardy, D. Kuh, T. Rochat, P.-O. Bridevaux, M. Eeftens, M.-Y. Tsai, S. Villani, H.C. Phuleria, M. Birk, J. Cyrys, M. Cirach, A. de Nazelle, M.J. Nieuwenhuijsen, B. Forsberg, K. de Hoogh, C. Declerq, R. Bono, P. Piccioni, U. Quass, J. Heinrich, D. Jarvis, I. Pin, R. Beelen, G. Hoek, B. Brunekreef, C. Schindler, J. Sunyer, U. Krämer, F. Kauffmann, A.L. Hansell, N. Künzli, N. Probst-Hensch, Adult lung function and long-term air pollution exposure. ESCAPE: a multicentre cohort study and meta-analysis, European Respiratory Journal, 45 (2015) 38-50.

[15] C.A. Pope, D.G. Renlund, A.G. Kfoury, H.T. May, B.D. Horne, Relation of Heart Failure Hospitalization to Exposure to Fine Particulate Air Pollution, The American Journal of Cardiology, 102 (2008) 1230-1234.
[16] B.A. Franklin, R. Brook, C. Arden Pope, Air Pollution and Cardiovascular Disease, Current Problems in Cardiology, 40 (2015) 207-238.
[17] WHO, Health aspects of air pollution with particulate matter, ozone and nitrogen dioxide : report on a WHO working group, Bonn, Germany 13-15 January, (2003).
[18] I. Manisalidis, E. Stavropoulou, A. Stavropoulos, E. Bezirtzoglou, Environmental and Health Impacts of Air Pollution: A Review, Frontiers in public health, 8 (2020) 14-14.
[19] D.A. Grantz, J.H.B. Garner, D.W. Johnson, Ecological effects of particulate matter, Environment International, 29 (2003) 213-239.
[20] S. Sobanska, G. Falgayrac, J. Rimetz-Planchon, E. Perdrix, C. Brémard, J. Barbillat, Resolving the internal structure of individual atmospheric aerosol particle by the combination of Atomic Force Microscopy, ESEM–EDX, Raman and ToF–SIMS imaging, Microchemical Journal, 114 (2014) 89-98.
[21] J.O. Cáceres, D. Sanz-Mangas, S. Manzoor, L.V. Pérez-Arribas, J. Anzano, Quantification of particulate matter, tracking the origin and relationship between elements for the environmental monitoring of the Antarctic region, Science of The Total Environment, 665 (2019) 125-132.
[22] C. Marina-Montes, L.V. Pérez-Arribas, M. Escudero, J. Anzano, J.O. Cáceres, Heavy metal transport and evolution of atmospheric aerosols in the Antarctic region, Science of The Total Environment, 721 (2020) 137702.
[23] C. Marina-Montes, L.V. Pérez-Arribas, J. Anzano, J.O. Cáceres, Local and Remote Sources of Airborne Suspended Particulate Matter in the Antarctic Region, Atmosphere, 11 (2020).
[24] L. Borgese, F. Bilo, A. Zacco, S. Federici, A.W. Mutahi, E. Bontempi, K. Trzepla, N. Hyslop, S. Yatkin, P. Wobrauschek, J. Prost, D. Ingerle, L.E. Depero, The assessment of a method for measurements and lead quantification in air particulate matter using total reflection X-ray fluorescence spectrometers, Spectrochimica Acta Part B: Atomic Spectroscopy, 167 (2020) 105840.
[25] V.L. Mateus, I.L.G. Monteiro, R.C.C. Rocha, T.D. Saint'Pierre, A. Gioda, Study of the chemical composition of particulate matter from the Rio de Janeiro metropolitan region, Brazil, by inductively coupled plasma-mass spectrometry and optical emission spectrometry, Spectrochimica Acta Part B: Atomic Spectroscopy, 86 (2013) 131-136.
[26] D. Diaz, D.W. Hahn, U. Panne, Chapter 22 - LIBS for aerosol analysis, in: J.P. Singh, S.N. Thakur (Eds.) Laser-Induced Breakdown Spectroscopy (Second Edition), Elsevier, Amsterdam, 2020, pp. 499-535.
[27] A.W. Miziolek, V. Palleschi, I. Schechter, Laser Induced Breakdown Spectroscopy (LIBS), 1 ed., Cambridge University Press, New York - USA, 2006.
[28] A.K. Rai, J.K. Pati, A.K. Rai, Chapter 16 - LIBS study of geological samples coupled with chemometric methods, in: J.P. Singh, S.N. Thakur (Eds.) Laser-Induced Breakdown Spectroscopy (Second Edition), Elsevier, Amsterdam, 2020, pp. 369-384.
[29] V. Motto-Ros, S. Moncayo, C. Fabre, B. Busser, Chapter 14 - LIBS imaging applications, in: J.P. Singh, S.N. Thakur (Eds.) Laser-Induced Breakdown Spectroscopy (Second Edition), Elsevier, Amsterdam, 2020, pp. 329-346.
[30] R.C. Wiens, X. Wan, J. Lasue, S. Maurice, Chapter 20 - Laser-induced breakdown spectroscopy in planetary science, in: J.P. Singh, S.N. Thakur (Eds.) Laser-Induced Breakdown Spectroscopy (Second Edition), Elsevier, Amsterdam, 2020, pp. 441-471.
[31] M.Z. Martin, M.-D. Cheng, R.C. Martin, Aerosol Measurement by Laser-Induced Plasma Technique: A Review, Aerosol Science and Technology, 31 (1999) 409-421.
[32] B.W. Smith, D.W. Hahn, E. Gibb, I. Gornushkin, J.D. Winefordner, Laser Induced Plasma Spectroscopy for the Characterization of Aerosols and Particulates, KONA Powder and Particle Journal, 19 (2001) 25-33.

[33] R.-J. Lasheras, D. Paules, M. Escudero, J. Anzano, S. Legnaioli, S. Pagnotta, V. Palleschi, Quantitative analysis of major components of mineral particulate matter by calibration free laser-induced breakdown spectroscopy, Spectrochimica Acta Part B: Atomic Spectroscopy, 171 (2020) 105918.
[34] J.O. Cáceres, F. Pelascini, V. Motto-Ros, S. Moncayo, F. Trichard, G. Panczer, A. Marín-Roldán, J.A. Cruz, I. Coronado, J. Martín-Chivelet, Megapixel multi-elemental imaging by Laser-Induced Breakdown Spectroscopy, a technology with considerable potential for paleoclimate studies, Scientific reports, 7 (2017) 5080-5080.
[35] C. Fabre, D. Devismes, S. Moncayo, F. Pelascini, F. Trichard, A. Lecomte, B. Bousquet, J. Cauzid, V. Motto-Ros, Elemental imaging by laser-induced breakdown spectroscopy for the geological characterization of minerals, Journal of Analytical Atomic Spectrometry, 33 (2018) 1345-1353.
[36] L. Jolivet, V. Motto-Ros, L. Sorbier, T. Sozinho, C.P. Lienemann, Quantitative imaging of carbon in heterogeneous refining catalysts, Journal of Analytical Atomic Spectrometry, 35 (2020) 896-903.
[37] U.-E. 12341, Standard Gravimetric Measurement Method for Determination of the PM10 or PM2.5 Mass Concentration of Suspended Particulate Matter., 2015.
[38] X. Querol, A. Alastuey, S. Rodriguez, F. Plana, C.R. Ruiz, N. Cots, G. Massagué, O. Puig, PM10 and PM2.5 source apportionment in the Barcelona Metropolitan area, Catalonia, Spain, Atmospheric Environment, 35 (2001) 6407-6419.
[39] Y. Gimenez, B. Busser, F. Trichard, A. Kulesza, J.M. Laurent, V. Zaun, F. Lux, J.M. Benoit, G. Panczer, P. Dugourd, O. Tillement, F. Pelascini, L. Sancey, V. Motto-Ros, 3D Imaging of Nanoparticle Distribution in Biological Tissue by Laser-Induced Breakdown Spectroscopy, Scientific Reports, 6 (2016) 29936.
[40] S. Moncayo, L. Duponchel, N. Mousavipak, G. Panczer, F. Trichard, B. Bousquet, F. Pelascini, V. Motto-Ros, Exploration of megapixel hyperspectral LIBS images using principal component analysis, Journal of Analytical Atomic Spectrometry, 33 (2018) 210-220.
[41] V. Motto-Ros, S. Moncayo, F. Trichard, F. Pelascini, Investigation of signal extraction in the frame of laser induced breakdown spectroscopy imaging, Spectrochimica Acta Part B: Atomic Spectroscopy, 155 (2019) 127-133.
[42] U. Panne, R.E. Neuhauser, M. Theisen, H. Fink, R. Niessner, Analysis of heavy metal aerosols on filters by laser-induced plasma spectroscopy, Spectrochimica Acta Part B: Atomic Spectroscopy, 56 (2001) 839-850.
[43] C.B. Stipe, A.L. Miller, J. Brown, E. Guevara, E. Cauda, Evaluation of Laser-Induced Breakdown Spectroscopy (LIBS) for Measurement of Silica on Filter Samples of Coal Dust, Applied Spectroscopy, 66 (2012) 1286-1293.
[44] L. Fierce, N. Riemer, T.C. Bond, Explaining variance in black carbon's aging timescale, Atmos. Chem. Phys., 15 (2015) 3173-3191.
[45] M.Z. Jacobson, Strong radiative heating due to the mixing state of black carbon in atmospheric aerosols, Nature, 409 (2001) 695-697.
[46] O.S. Ryder, A.P. Ault, J.F. Cahill, T.L. Guasco, T.P. Riedel, L.A. Cuadra-Rodriguez, C.J. Gaston, E. Fitzgerald, C. Lee, K.A. Prather, T.H. Bertram, On the Role of Particle Inorganic Mixing State in the Reactive Uptake of N2O5 to Ambient Aerosol Particles, Environmental Science & Technology, 48 (2014) 1618-1627.